Analysis of the Electrical Conduction in Percolative Nanocomposites Based on Castor-Oil Polyurethane with Carbon Black and Activated Carbon Nanopowder

Paulo Vinícius Rebeque,[1] Michael Jones Silva,[2] Cicero Rafael Cena,[3] Haroldo Naoyuki Nagashima,[4] José Antônio Malmonge,[4] Darcy Hiroe Fujii Kanda[4]

[1]*Instituto Federal do Rio Grande do Sul (IFRS), Bento Gonçalves, RS, Brazil*

[2]*Universidade Estadual Paulista (Unesp), Campus de Rosana, Rosana, SP, Brazil*

[3]*Instituto de Física, Universidade Federal de Mato Grosso do Sul (UFMS), Campo Grande, MS, Brazil*

[4]*Departamento de Física e Química, Universidade Estadual Paulista (Unesp), Faculdade de Engenharia, Ilha Solteira, SP, Brazil*

Flexible nanocomposite films derived from castor-oil polyurethane (PUR) and conductive fillers of activated carbon nanopowder (CNP) and carbon black (CB) nanoparticles were prepared by casting and characterized by scanning electron microscopy (SEM) as well as direct (dc) and alternate current (ac) electrical conductivity measurements. The fillers exhibited spherical morphology with diameters ranging between 40 and 60 nm. Compared to CNP, CB was dispersed better in the matrix. Based on the classical percolation theory, different universal exponents were obtained from the conductivity curve analysis. The PUR/CNP nanocomposite obeyed the universal percolation theory, while the PUR/CB nanocomposite did not obey it. The PUR/CNP nanocomposites exhibited a higher percolation threshold ($p_c = 29.3$ vol%) and lower dc conductivity compared to PUR/CB nanocomposites ($p_c = 5.7$ vol%). This difference is related to the physics and chemical characteristics of the CNP and CB filler dispersed in the matrix. The ac conductivity of the nanocomposites was described by the Jonscher power law confirmed that conduction occurs through a hopping mechanism between localized hopping. **POLYM. COMPOS., 40:7–15, 2019.** **© 2017 Society of Plastics Engineers**

INTRODUCTION

Conventional polymers are considered as electrically insulating materials because of the low concentration of free charge carriers. However, their electrical conductivity can be modified by the incorporation of a conductive filler, for example, semiconductor or conductor particles and conducting polymers. Conductive polymer composites (CPCs) are prepared from a conventional polymer and a conductive filler, permitting the combination of the excellent mechanical properties, flexibility, and facile processing ability of polymeric materials with a better electrical property of the conducting particles. CPCs are considered disordered materials, and their electrical conductivity depends on different factors, for example, preparation method (amount and distribution of the dispersed filler in the host matrix), volume fraction, and phase conductivity [1, 2]. For example, in case of an extremely low conductive filler concentration, there is a considerable distance between the particles; hence, the conductivity of the composite is approximately similar to that of the polymeric matrix [3]. On the other hand, in case of a high conducting filler concentration, an insulator–metal transition occurs, leading to a continuous conducting path in the conductive fillers [4]. At this stage, a percolation threshold is observed, and the conductivity (σ) of the composite abruptly increases [5–7].

The conduction in CPCs is determined by two main mechanisms, percolation model for hopping and tunneling conduction, respectively. In the percolation model for hopping conduction, the conductive fillers are in physical contact, forming a three-dimensional structure in which the charge carriers jump between localized states within the bulk of the composite. On the other hand, in the percolation model for tunneling conduction, the conductive fillers are separated by a thin insulating layer or a barrier potential [8, 9].

Correspondence to: M. J. Silva; e-mail: michael@rosana.unesp.br
DOI 10.1002/pc.24588
Published online in Wiley Online Library (wileyonlinelibrary.com).

It is crucial to examine the electrical properties of CPCs because of their immense potential for technological applications, for example, gas sensing, antistatic shielding, electronic and food packaging, and electromagnetic radiation shielding, as well as in the electronics and aerospace industries. Several studies have reported the preparation of CPCs from carbon black (CB), carbon nanotubes, carbon fibers, and activated carbon nanopowder (CNP), and the potential of a carbon-based filler to improve the electrical properties of the insulator polymer matrix has been demonstrated [10–29]. However, few studies have reported the electrical properties of CPCs based on biopolymers, such as castor-oil polyurethane (PUR) with CB and CNP fillers.

The reaction between diisocyanates and polyols leads to the formation of polyurethanes (PU), which have a urethane linkage [30]. PUs are classified as multiblock copolymers because the polymer chain consists of blocks of hard and soft segments, which permits the control of their flexibility, hardness, and mechanical properties [31–34]. PUR is extracted from the castor bean seed, a native Brazilian plant. This biopolymer is obtained by mixing the pre-polymer and the castor-oil-derived polyol. This biopolymer exhibits properties, for example, flexibility, lightweight nature, and mechanical properties, comparable to synthetic PU; these properties can be controlled according to the pre-polymer/polyol ratio [35].

In this study, flexible thick films of nanocomposites based on a biopolymer (PUR) filled with CB and CNPs, with potential applications as electrostatic dissipative devices, were produced by casting. Their electrical properties were evaluated by direct current (dc) electrical conductivity and impedance spectroscopy measurements, and their electrical conductivity and conduction were evaluated as function of the particle concentration and applied external electric field frequency. Significant differences in the electrical properties of the nanocomposites were observed depending on the filler used, that is, CB or CNP. Besides of the filler conductive properties, this behavior can be mainly related to the dispersion of the filler in the PUR matrix.

EXPERIMENTAL

Preparation of the PUR/CNP and PUR/CB Nanocomposites

Materials. PUR was obtained at a 1.0:0.7 molar ratio for the pre-polymer F-329 (derived from isocyanate) to polyol 21 L (derived from castor oil), and all reagents were provided by the Analytical Chemistry and Polymer Technology Group (University of São Paulo, USP). CNP and CB (*XE2*/*PRINTEX*) were purchased from Sigma-Aldrich Inc. and Degussa LTDA, respectively. Table 1 summarizes the particle size, surface area, and density of the conductive fillers, supplied by the respective manufacturers.

TABLE 1. Particle size, surface area, density, and electrical conductivity of the CNP and CB nanoparticles.

Parameters	CNP	CB
Particle size (nm)	50	35
Surface area (m^2/g)	100	1,000
Density (g/cm^3)	0.336	0.1
Electrical conductivity (S/m)	27.0	200.0

Sample Preparation. PUR/CB and PUR/CNP samples were obtained by mixing the pre-polymer (2.0 g) and polyol (1.4 g) in a 5.0 mL of chloroform under constant stirring, and different concentrations (5–40 vol%) of the conductive filler (*i.e.*, CB or CNP) were dispersed into the solution in desired proportions. Flexible nanocomposite films, with thickness ranging from 80 to 150 μm, were obtained by casting the PUR/CB and PUR/CNP mixtures, followed by the deposition on glass slides and curing at room temperature for 2 days. The conductive filler mass, employed in each sample, was determined according to *Eq. 1*. Table 2 summarizes the amount of materials used

$$m_x = m_{PUR}\frac{\rho_x \cdot \phi_x}{\rho_{PUR} \cdot (1-\phi_x)} \quad (1)$$

where m_{PUR} and ρ_{PUR} represent the mass and density of PUR, respectively. m_x, ρ_x, and ϕ_x represent the mass, density, and volume fraction of CNP or CB, respectively.

Characterization

Current–Voltage Measurements. The dc conductivity was measured by the two-probe method by using a programmable voltage-current source (KEITHLEY, model 236). Gold electrodes were evaporated on both faces of the films for electrical contact. The dc electrical conductivity was calculated using *Eq. 2*

$$\sigma_{dc} = \frac{L}{R \cdot A} \quad (2)$$

where R is the ohmic resistance (obtained from slope of the I vs. V graph), A is the electrode area, and L is the sample thickness.

TABLE 2. Masses of CNP and CB and their respective volume fractions (in 3.4 g of PUR).

vol%	Mass of CB (g)	Mass of CNP (g)
5	0.017	0.060
10	0.037	0.127
15	0.060	0.202
20	0.085	0.287
25	0.113	0.381
30	0.146	0.489
35	0.183	0.615
40	0.227	0.762

DOI 10.1002/pc

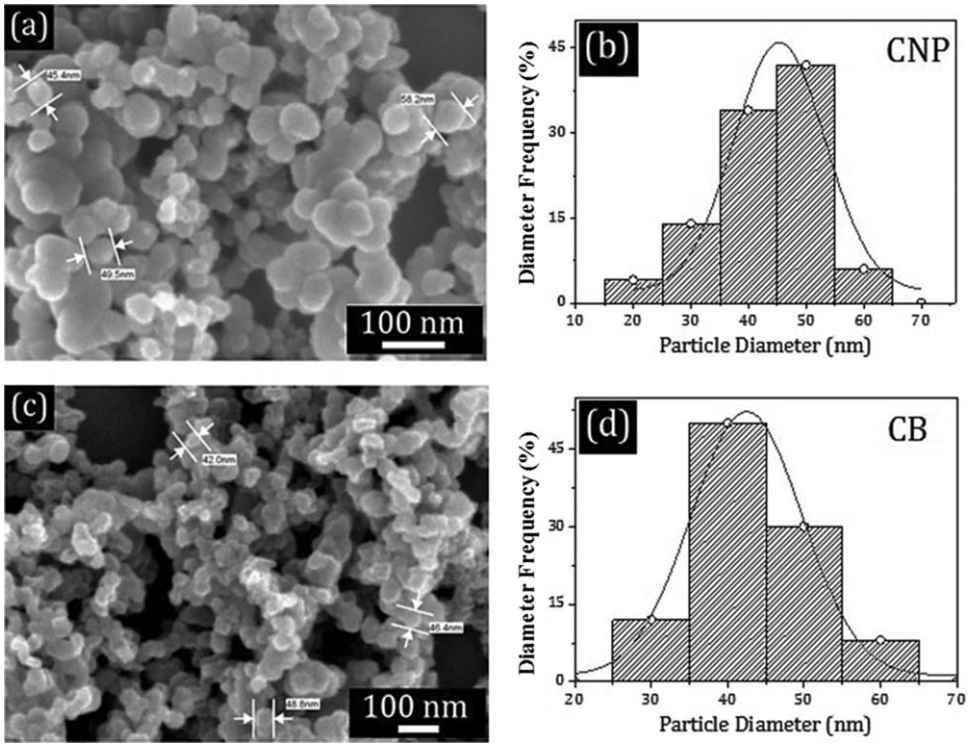

FIG. 1. FEG-SEM images of the (a and b) CNP particles and (c and d) CB particles and their respective histograms of the particle size distribution.

Impedance Spectroscopy. Alternate current (ac) electrical conductivity was measured at room temperature at frequencies ranging from 100 Hz to 1 MHz using an impedance analyzer from Hewlett Packard (model 4192A). The ac complex electrical conductivity was calculated using *Eq. 3*

$$\sigma^* = \frac{L \cdot Z'}{A \cdot (Z'^2 + Z''^2)} + \frac{L \cdot Z''}{A \cdot (Z'^2 + Z''^2)} \quad (3)$$

where A is the electrode area, L is the sample thickness, Z' and Z'' are the real and the imaginary parts of the complex impedance, respectively.

Field-Emission Scanning Electron Microscopy (FEG-SEM). The morphology of the nanocomposites was analyzed using a Supra 35 field-emission scanning electron microscopy instrument (Zeiss). The nanocomposites were fractured after immersion in liquid nitrogen and dried under dynamic vacuum for 1 h. Next, the fractured transverse sections of the samples were coated with carbon.

RESULTS AND DISCUSSION

Morphology

Figure 1 shows the typical grain morphology of the CB and CNP nanoparticles used as the conductive phase in the polymeric matrix. CB and CNP particles exhibited similar spherical morphology, with a diameter distribution ranging from 20 to 60 nm. The inset of the figure showed CNP and CB particles, with average diameters of around 45 and 40 nm, respectively. These values are similar to those provided by the manufacturers.

Figure 2 shows the cross sections of the PUR/CNP and PUR/CB thick film composites with the introduction of 30 vol% of nanoparticles. CNP and CB nanoparticles exhibited a homogeneous distribution pattern with different phases in the nanocomposite. However, CB particles (Fig. 2c) were better dispersed than CNP particles (Fig. 2a). In the PUR/CNP nanocomposite, the CNP particles tend to cluster more in certain regions of the matrix, separated by large insulating regions which interfere during the conduction of charge carriers. On the other hand, the CB particles were distributed better than the CNP particles, facilitating electrical conduction.

CB and CNP exhibit different chemical and physical characteristics. CB is virtually pure elemental carbon in the form of colloidal particles, which is produced by the incomplete combustion or cracking of heavy petroleum products, gases, and vapors under controlled conditions. Activated carbon, which is physically different from CB, is obtained from charcoal; it contains pores that can adsorb heavy metals, poison, and dirt particles, for example, in water filtration [36, 37].

Carbon-based materials exhibit four fundamental properties that determine their potential for different applications, (i) thickness, (ii) particle size, (iii) internal particle

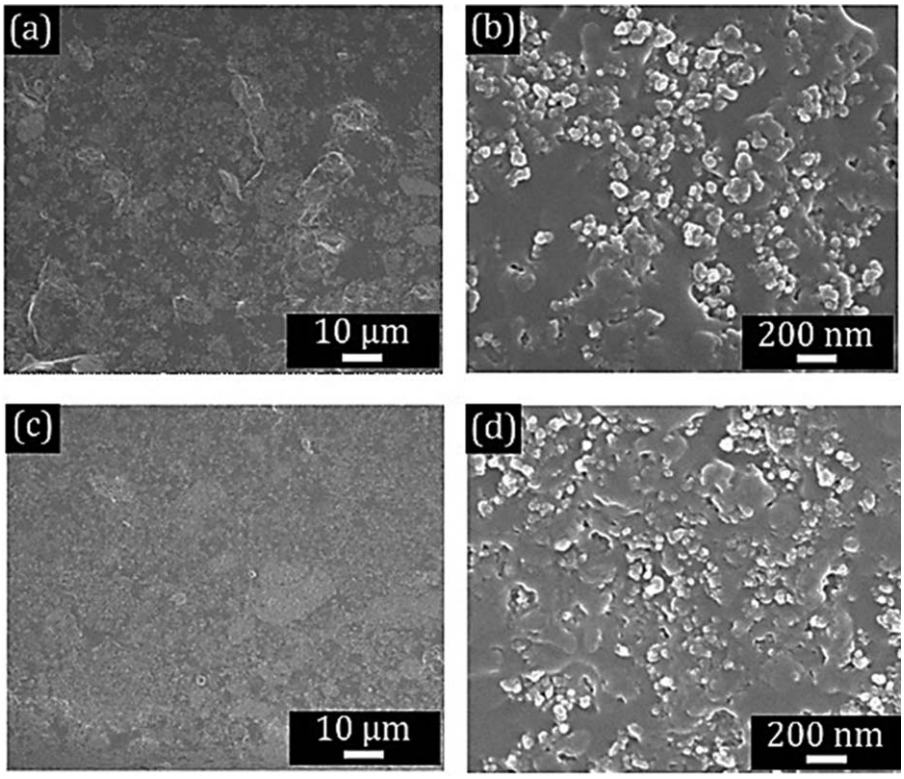

FIG. 2. FEG-SEM images of the (a and b) PUR/CNP composites and (c and d) PUR/CB with 30 vol% of nanoparticles added to the polymeric matrix.

structure, which determines their aggregation, dispersion behavior, and electrical conductivity, and (iv) surface functionality, affecting their wettability, viscosity, and electrical conductivity, respectively [36]. CNP particles exhibited more surface functionalities and higher particle size distribution and density compared to CB particles. From the physical and chemical characteristics as well as their synthesis, CNPs tended to aggregate because of their intrinsic van der Waal interactions, leading to their decreased dispersion [38].

Papers in the literature have demonstrated the good dispersion of CB and CNP-based polymer composite. Deniz et al. [25] has observed that the CB particles presents good dispersion and interaction with the polyvinyl fluoride (PVDF), the fillers with spherical morphology showed to a small clusters formation separated by the PVDF matrix. Similar behavior has been observed by Arora et al. [27] which carried out a study of the chemical and physical properties of the acrylic resin/activated carbon composite.

Electrical Conductivity Analysis

The dc Electrical Conductivity. The dc electrical conductivity measurements were carried out to examine the effect of the conductive filler on the electrical properties of the nanocomposites. Figure 3 plots the dc conductivity (σ_{dc}) as a function of the CNP and CB volume fraction of the nanocomposite samples. As can be observed from Fig. 3, the percolation threshold was around 5.7 vol% for PUR/CB and 29.3 vol% PUR/CNP. Above the percolation threshold the σ_{dc} of the PUR/CNP and PUR/CB nanocomposites were 10^{-6} and 10^{-4} S/m respectively, these values are 6 and 8 orders of magnitude higher than the σ_{dc} of the neat PUR.

The comparison of the two nanocomposites revealed that PUR/CB exhibits higher conductivity and a lower percolation threshold compared to PUR/CNP. This result is in agreement with the scanning electron microscopy FEG-SEM images shown in Fig. 2. CNP particles tended to clump together, thereby forming isolated islands that are separated by large insulating regions (PUR matrix); on the other hand, CB particles were better dispersed, forming a network of conducting islands within the nanocomposite with a lower amount of CB than CNP. This behavior is mainly related to its higher density and particle size distribution, pore structure, and functionalized surface characteristics, which affect the dispersion within the matrix and electrical conductivity of the PUR/CNP nanocomposite [39]. A comparative analysis reveals that the electrical conductivity obtained for the nanocomposites of the present work is close to those mentioned in the literature. Arora et al. [27] studied the electrical properties of acrylic resin/activated carbon composites and reported the electrical conductivity of approximately 10^{-4} S/m with the addition of 30 wt% activated carbon. Cheng

 DOI 10.1002/pc

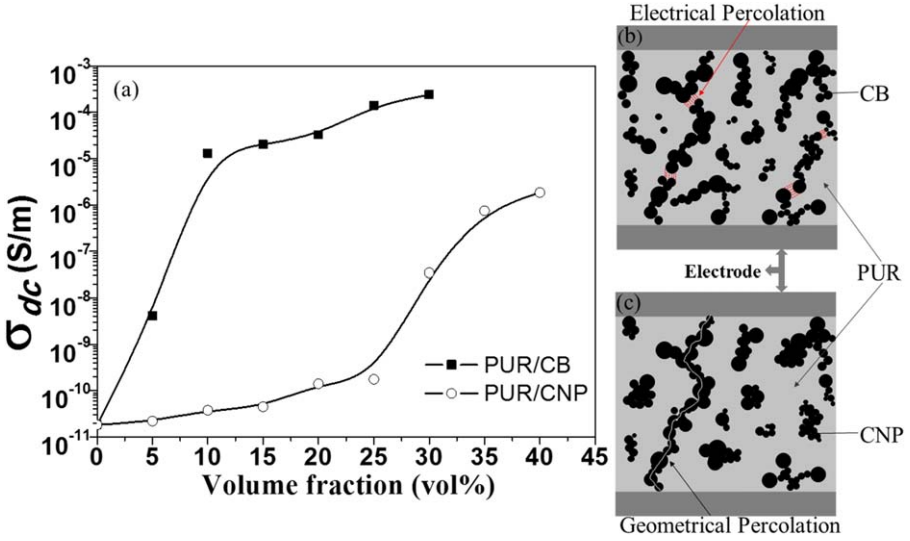

FIG. 3. (a) dc electrical conductivity as a function of the CNP and CB volume fractions. (b) Electrical percolation in PUR/CB. (c) Geometrical percolation (by physical contact) in PUR/CNP. [Color figure can be viewed at wileyonlinelibrary.com]

et al. [28] obtained binary composite of polyamide 6 filled with CB, and multiwalled carbon nanotubes (MWCNTs), the electrical conductivity value were 0.5 and 0.04 S/m, respectively. Although electrical conductivity of MWCNTs is higher than CB, the authors observed that CB/PA6 binary composite have higher conductivity than MWCNT/PA6 binary composite. [28] This behavior was mainly related to the physical and chemical characteristics of the filler. CB particles have the highest surface energy and the relatively highest electrical conductivity while MWCNTs exhibit the highest aspect ratio and excellent electrical conductivity [28]. However, due to the agglomeration of MWCNTs resulted from the strong van der Waal forces among them and the high viscosity of MWCNT/PA6

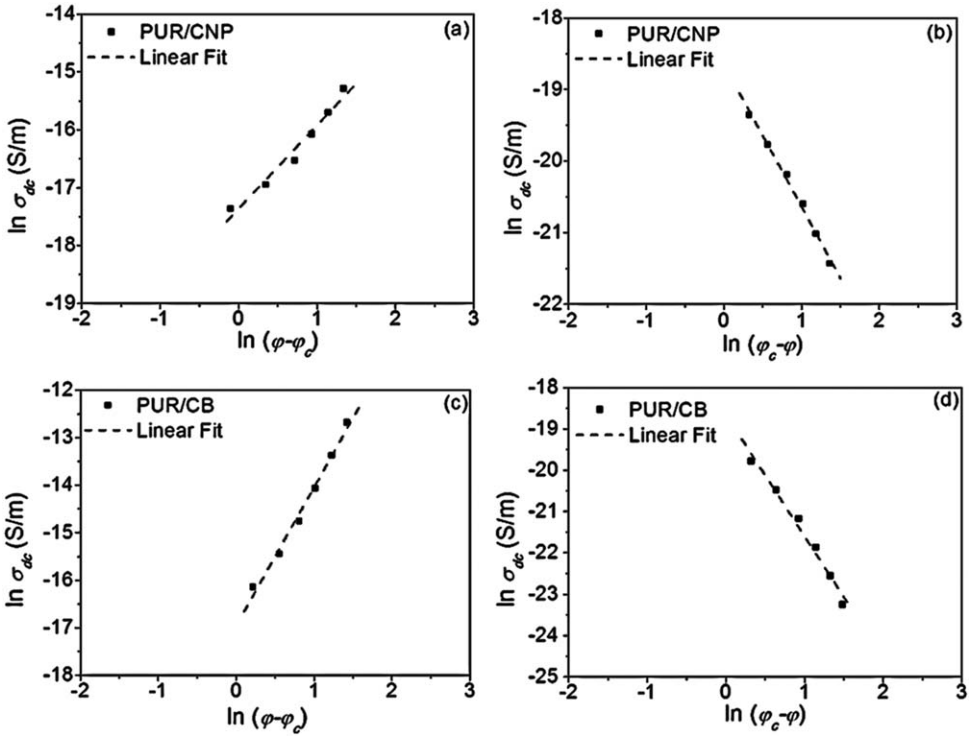

FIG. 4. Double-logarithmic plot according to *Eq. 4* (a) and (c); *Eq. 5* (b) and (d). (a and b) PUR/CNP samples; (c and d) PUR/CB samples.

TABLE 3. Parameters obtained from linear fit using *Eqs.* 4 and 5 for the PUR/CNP and PUR/CB nanocomposites.

Parameters	k (S/m)	q (S/m)	t	s
PUR/CNP	2.92×10^{-8}	7.95×10^{-9}	1.53	−1.99
PUR/CB	4.39×10^{-8}	7.87×10^{-9}	2.91	−2.94

composite during the compounding process, MWCNT-based composites have a major drawback in conduction of electricity [28]. On the other hand, due to the inherent structure of CB, it is possible to form a 3D network in the polymer matrix [28].

By the percolation theory, when the volume fraction of the conductive filler reaches the percolation threshold, an infinite conductive path will be created inside the composite, which facilitates the movement of the charge carriers. Hence, the conductivity abruptly increases. The percolation theory predicts that conductivity obeys a power law for systems formed by insulating and conductive phases [1, 5, 8]. The σ_{dc} behavior for systems with a volume fraction of conductive particles above the percolation threshold is described by *Eq. 4*

$$\sigma \approx k(\varphi - \varphi_c)^t \tag{4}$$

where φ is the conducting phase, φ_c is the critical volume (percolation threshold) at which the insulator to conductor transition occurs, and t is the conductivity critical exponent. Similarly, the conductivity of systems with a volume fraction less than the percolation threshold is given by *Eq. 5*

$$\sigma \approx q(\varphi_c - \varphi)^s \tag{5}$$

where s is the conductivity critical exponent, and q is a constant.

Figure 4 plots ln (σ_{dc}) versus ln ($\varphi - \varphi_c$) and ln (σ_{dc}) versus ln ($\varphi_c - \varphi$) for PUR/CB and PUR/CNP nanocomposites according to *Eqs. 4* and *5*, respectively, to estimate the critical exponent (t and s) and constant (k and q). The critical exponent and constant values were estimated by fitting the data shown in Fig. 4. Table 3 summarizes these values.

The critical exponent values for the PUR/CNP nanocomposites were in agreement with the universal percolation theory, which predicts a range of 1.5–2.0 for s. The conduction of charge carriers occurs through an infinite three-dimensional network, which is formed by the physical contact of the CNP nanoparticle agglomerates (Fig. 1c). However, the critical exponent values for the PUR/CB nanocomposite were not in agreement with the universal percolation theory. A similar behavior has been reported previously [40, 41]. In this case, the conductive filler or clusters are sufficiently near to facilitate conduction, the hopping and tunneling of the charge carriers occur between the neighboring conductive fillers (Fig. 1b).

The ac Complex Electrical Conductivity. Figure 5 shows the real ($\sigma'(\omega)$) and imaginary parts ($\sigma''(\omega)$) of the complex conductivity as a function of the frequency for the PUR/CNP and PUR/CB nanocomposites. The complex conductivity for both nanocomposites was similar to

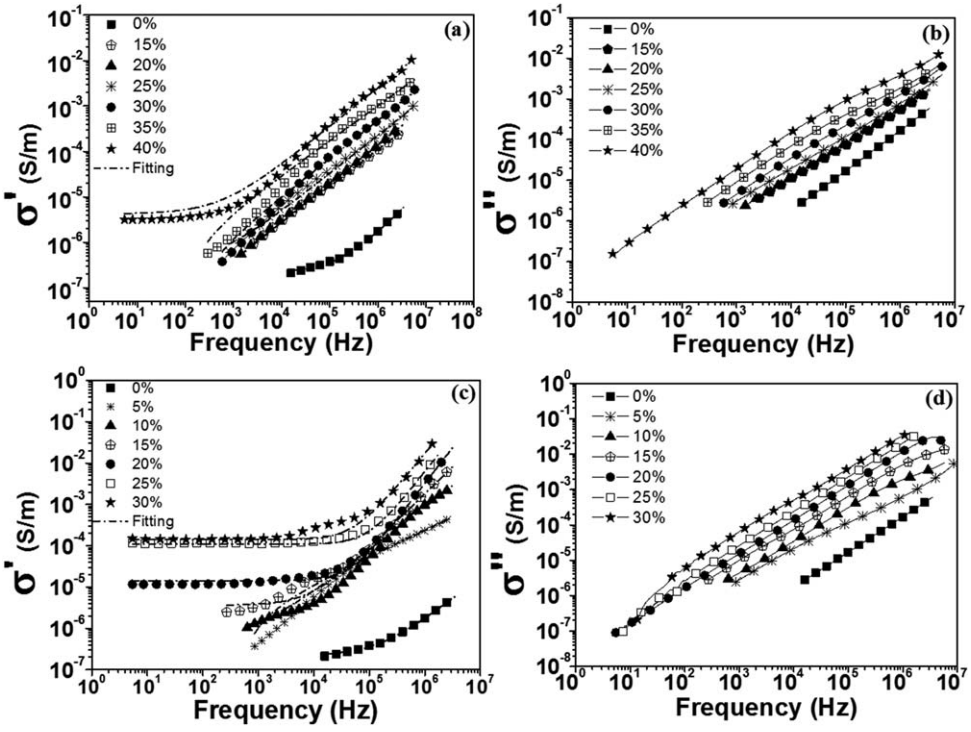

FIG. 5. The ac complex conductivity as a function of frequency for (a and b) PUR/CNP and (c and d) PUR/CB with different volume fractions of the conductive filler.

 DOI 10.1002/pc

TABLE 4. Parameters obtained from fitting of the experimental data using the Jonscher's equation for the PUR/CNP and PUR/CB nanocomposites and neat PUR.

Samples	σ_{dc} (S/m)	A	n
PUR	2.16×10^{-7}	9.54×10^{-13}	1.032
PUR/CNP (85/15)	1.09×10^{-6}	1.52×10^{-10}	0.90
PUR/CNP (80/20)	2.18×10^{-6}	4.35×10^{-10}	0.91
PUR/CNP (75/25)	7.98×10^{-6}	6.56×10^{-10}	0.91
PUR/CNP (70/30)	1.04×10^{-5}	2.19×10^{-9}	0.88
PUR/CNP (65/35)	1.25×10^{-5}	1.71×10^{-9}	0.79
PUR/CNP (60/40)	5.09×10^{-5}	6.63×10^{-9}	0.85
PUR/CB (95/05)	3.17×10^{-7}	3.73×10^{-11}	1.02
PUR/CB (90/10)	7.72×10^{-7}	5.68×10^{-11}	1.10
PUR/CB (85/15)	3.67×10^{-6}	2.66×10^{-11}	1.30
PUR/CB (80/20)	1.43×10^{-5}	1.28×10^{-13}	1.73
PUR/CB (75/25)	1.11×10^{-4}	3.04×10^{-13}	1.71
PUR/CB (70/30)	1.39×10^{-4}	4.24×10^{-12}	1.60

that for disordered solids [8]. At above the percolation threshold, the samples exhibited two well-defined regions in the curve of $\sigma'(\omega)$. In the first region, ac conductivity exhibits a plateau at low frequencies, while in the second region it shows a frequency-dependent behavior at high frequencies. The critical frequency represents the stage at which the transition between the different regions occurs. Below the critical frequency, the conductivity is approximately equal to σ_{dc}.

At low frequencies, the charge carriers scan a large distance inside the composite before the direction of the electric field is changed; in this case, the mean distance covered by the charge carriers at frequencies less than the critical frequency is greater than the correlation length (size of the largest finite-size cluster); hence, conductivity is independent of the frequency [42]. Although at high frequency, the conduction of the charge carriers occurs by hopping between the localized states; hence, an almost linear increase in $\sigma'(\omega)$ is observed [43]. The ac conductivity in disordered solids $\sigma'(\omega)$ exhibits universal behavior, which can be described by the Jonscher power law and expressed as follows:[44, 45]

$$\sigma' = \sigma_{dc} + \sigma_{ac} = \sigma_{dc} + A\omega^n \quad (5)$$

where σ_{dc} is the dc conductivity (frequency-independent behavior), ω is the angular frequency of the applied electric field ($\omega = 2\pi\int$), A is the pre-exponential factor, and n is the fractional exponent. The n value represents the degree of interaction between the charge carriers and the surrounding environment; typically, this universal behavior of the n value ranges between 0 and 1, suggesting that conduction occurs through hopping [46, 47]. On the other hand, several previous studies have reported n values greater than 1 [48–52]. According to Papathanassiou et al.,[50] there is no physical argument to restrict the n value to less than 1 at the empirical universal law of Jonscher.

Table 4 summarizes the A and n values, which are obtained by fitting *Eq. 5* from the plot of log $\sigma'(\omega)$ versus log frequency for all of the PUR/CNP and PUR/CB nanocomposites. The n value for the PUR/CNP nanocomposite ranged between 0.7 and 1.0, while that for the PUR/CB nanocomposite ranged between 1.0 and 1.73 (Fig. 5). According to the n values obtained for both samples, the characteristic behavior of charge conduction involves hopping between localized states inside the conductive filler. Figure 5a,c shows the mathematical fitting by using *Eq. 5*, confirming the validity of the model for all samples at high frequencies. For the PUR/CNP and PUR/CB nanocomposite in which the concentration of the conductive filler is less than the percolation threshold, a frequency-dependent behavior was observed, which was described by the power law (*Eq. 5*). The main conduction mechanism is related to the dipole movement of the polymer chains and spatial charges trapped at the interfaces between the matrix and conductive clusters.

The imaginary part of conductivity ($\sigma''(\omega)$) at all concentrations of CNP or CB exhibited frequency-dependent behavior (Fig. 5b,d). Imaginary conductivity was proportional to the imaginary impedance (*Eq. 3*); hence, it is associated with the energy-dissipation effects of the material. As can be observed from Fig. 5b,d, the $\sigma''(\omega)$ behavior was independent of the conductive filler, but it increases with increasing frequency of the alternating

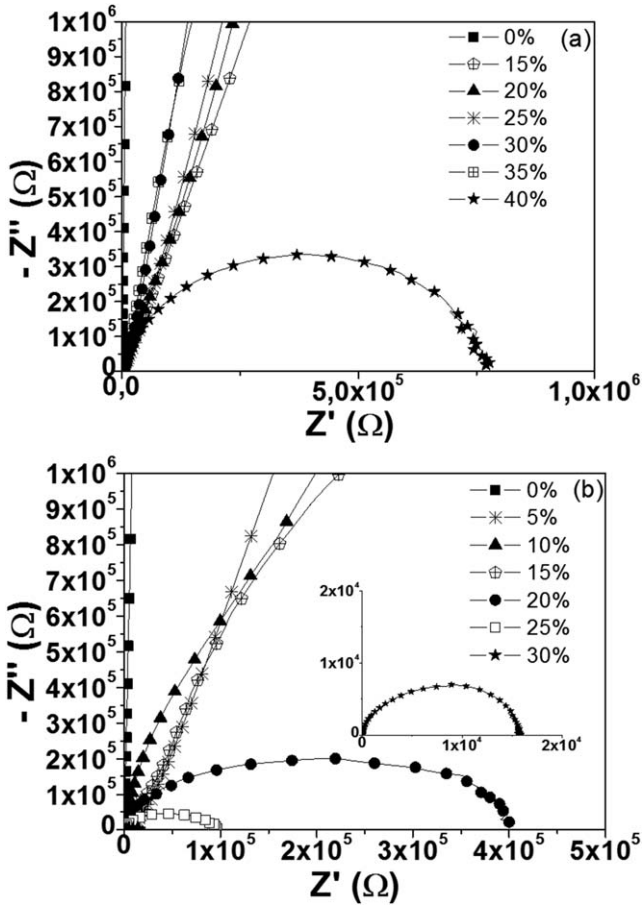

FIG. 6. Nyquist plot of the (a) PUR/CNP and (b) PUR/CB samples at different volume fractions of the conductive filler.

electric field. In addition, $\sigma''(\omega)$ increased with the increase in the CNP or CB volume fraction, related to the high number of charge carriers that participate during conduction; similarly, energy dissipation is observed.

Figure 6 shows the complex impedance spectrum or Nyquist plot (Z'' vs. Z') of the PUR composites at various CNP and CB concentrations at room temperature. In the typical Nyquist plot of the samples with CNP and CB concentrations greater than the percolation threshold, a broad semicircle was obtained for the entire frequency range examined; this behavior indicated that a single conduction mechanism is applicable in CNP [53]. An almost perfect semicircle for conductive samples suggested that it obeyed the Debye relaxation model. The semicircle gradually decreased with increasing conductive filler concentration, suggesting that the conductivity of the samples increases. The high-frequency semicircle observed for the samples in which the CNP and CB concentrations were greater than the percolation threshold is mainly related to the material bulk properties.

CONCLUSIONS

Flexible nanocomposites based on castor-oil-based PU were obtained with different content of CNP and CB nanoparticles by casting. Morphological characterization of the nanocomposites revealed that CB particles exhibit better dispersion compared to CNP particles.

The percolation threshold (p_c) values were 5.7 and 29.3 vol% for PUR/CB and PUR/CNP, respectively. The PUR/CB samples exhibited higher dc conductivity compared to PUR/CNP samples. The critical exponent values for the PUR/CNP nanocomposites were in agreement with the universal percolation theory; on the other hand, the nonuniversal critical exponent for the PUR/CB samples is associated with electrical percolation. The exponent n values obtained from the Jonscher power law confirmed that transport in the PUR/CNP nanocomposites occurs via a hopping mechanism. The exponent $n > 1$ was observed for the PUR/CB nanocomposite, indicating that the conduction occurs by localized hopping without leaving the surrounding of CB. CB exhibited a better impact on the electrical properties of the matrix compared to CNP particles, demonstrating its potential as conductive fillers, electrostatic dissipating devices, and antistatic flooring and coating materials.

REFERENCES

1. R. Strümpler and J. Glatz-Reichenbach, *J. Electroceram*, **3**, 329 (1999).
2. H. Bakkali, M. Dominguez, X. Batlle, and A. Labarta, *Scientific. Rep.*, **6**, 1 (2016).
3. A. Bunde and W. Dieterich, *J. Electroceram*, **5**, 81 (2000).
4. C.W. Nan, Y. Shen, and J. Ma, *Annu. Rev. Mater. Res.*, **40**, 131 (2010).
5. D. Stauffer and A. Aharony, *Introduction to Percolation Theory*. 2. rev. ed., Taylor & Francis, London, (2003).
6. Q.Q. Yang and J.Z. Liang, *Appl. Phys. Lett.*, **93**, 131918 (2008).
7. J. Liang and Q. Yang, *J. Appl. Phys.*, **102**, 083508 (2007).
8. M.J. Silva, D.H.F. Kanda, and H.N. Nagashima, *J. Non-Cryst. Solid.*, **358**, 270 (2012).
9. J.C. Huang, *Adv. Polym. Tech.*, **21**, 299 (2002).
10. H. Stoyanov, D. Mc Carthy, M. Kollosche, and G. Kofod, *Appl. Phys. Lett.*, **94**, 232905 (2009).
11. H. Zois, L. Apekis, and M. Omastová, *Macromol. Symp.*, **170**, 249 (2001).
12. M. Nanda, R.N.P. Chaudhary, and D.K. Tripathy, *Polym. Compos.*, **10**, 152 (2010).
13. F. Li, L. Qi, J. Yang, M. Xu, X. Luo, and D. Ma, *J. Appl. Polym. Sci.*, **75**, 68 (2000).
14. P.M. Ajayan and J.M. Tour, *Nature*, **447**, 1066 (2007).
15. A. Mierczynska, M. Mayne-L'Hermite, G. Boiteux, and J.K. Jeszka, *J. Appl. Polym. Sci.*, **105**, 158 (2007).
16. Q. Chen, Y. Xi, Y. Bin, and M. Matsuo, *J. Polym. Sci. Part. B*, **46**, 359 (2008).
17. B. Guiffard, L. Seveyrat, G. Sebald, and D. Guyomar, *J. Phys. D*, **39**, 3053 (2006).
18. L. Petit, B. Guiffard, L. Seveyrat, and D. Guyomar, *Sensor Actuat. A-Phys.*, **148**, 105 (2008).
19. A. Barroso-Bogeat, M. Alexandre-Franco, C. Fernández-González, A. Macías-García, and V. Gómez-Serrano, *Micropor. Mesopor. Mat.*, **209**, 90 (2015).
20. A.O. Sanches, D.H.F. Kanda, L.F. Malmonge, M.J. da Silva, W.K. Sakamoto, and J.A. Malmonge, *Polym. Test*, **60**, 253 (2017).
21. Z.Y. Xiong, B.Y. Zhang, L. Wang, J. Yu, and Z.X. Guo, *Carbon*, **70**, 233 (2014).
22. C. Schütter, C. Ramirez-Castro, M. Oljaca, S. Passerini, M. Winter, and A. Balducci, *J. Electrochem. Soc.*, **162**, A44 (2015).
23. A. Borenstein, O. Hanna, R. Attias, S. Luski, T. Brousse, and D. Aurbach, *J. Mater. Chem. A*, **5**, 12653 (2017).
24. X. Wang, E.N. Kalali, J.T. Wan, and D.Y. Wang, *Prog. Polym. Sci.*, **69**, 22 (2017).
25. W.D.S. Deniz, E.A. Sousa, E.P.S. Arlindo, W.K. Sakamoto, and G.C. Fuzari, *Polym. Bull.*, **72**, 1787 (2015).
26. X. Ding, J. Wang, S. Zhang, J. Wang, and S. Li, *Polym. Bull.*, **73**, 369 (2016).
27. M. Arora, C. Puri, M.A. Wahab, and P. Saini, *Indian J. Pure Appl. Phys.*, **52**, 251 (2014).
28. H.K.F. Cheng, N.G. Sahoo, Y. Pan, L. Li, S.H. Chan, J. Zhao, and G. Chen, *J. Polym. Sci. Pol. Phys.*, **48**, 1203 (2010).
29. J. Javad, and A.A. Katbab, *Polym. Compos.*, 1 (2017).
30. C. Hepburn, *Iran J. Polym. Sci. Tecnol.*, **1**, 84 (1992).
31. D.M. Crawford, R.G. Bass, and T.W. Haas, *Thermochim. Acta*, **323**, 56 (1998).
32. W.K. Sakamoto, D.H.F. Kanda, and F.A. Andrade, *J. Mater. Sci.*, **38**, 1465 (2003).
33. W.F. Alves, D.H. Kanda, L.F. Malmonge, J.A. Malmonge, and L.H. Mattoso, *J. Appl. Polym. Sci.*, **105**, 706 (2006).

34. A.O. Sanches, L.H.S. Ricco, L.F. Malmonge, M.J. Silva, W.K. Sakamoto, and J.A. Malmonge, *Polym. Test*, **40**, 99 (2014).
35. D.H.F. Kanda, H.N. Nagashima, J.A. Malmonge, W.K. Sakamoto, and G.O. Chierice, *J. Mater. Sci*., **43**, 5436 (2008).
36. H. Marsh and F.R. Reinoso, *Activated Carbon*. Elsevier, Amsterdam (2006).
37. J.L. Anderson, "Advanced Technologies for Lead–Acid Rechargeable Batteries," in *Electrochemical Energy: Advanced Materials and Technologies*, Vol. **1**, P.K. Shen, C.Y. Wang, S.P. Jiang, X. Sun, and J. Zhang, Eds., Electrochemical Energy: Advanced Materials and Technologies, CRC Press, 219 New York (2015).
38. T. Kaur and A. Thirugnanam, *J. Mater. Sci. Technol*., **1**, 1 (2016).
39. R.A. Antunes, M.C.L. de Oliveira, G. Ett, and V. Ett, *J. Power Sources*, **196**, 2945 (2011).
40. M.J. Silva, A.O. Sanches, L.F. Malmonge, and J.A. Malmonge, *Mater. Res*., **17**, 59 (2014).
41. M.B. Heaney, *Phys. Rev. B*, **52**, 12477 (1995).
42. B.E. Kilbride, J.N. Coleman, J. Fraysse, P. Fournet, M. Cadek, A. Drury, S. Hutzler, S. Roth, and W.J. Blau, *J. Appl. Phys*., **92**, 4024 (2002).
43. S. Sinha, S.K. Chatterjee, J. Ghosh, and A.K. Meikap, *Polym. Compos*., **38**, 287 (2015).
44. B.M. Greenhoe, M.K. Hassan, J.S. Wiggins, and K.A. Mauritz, *J. Polym. Sci. Part B*, **54**, 1918 (2016).
45. S. Barrau, P. Demont, A. Peigney, C. Laurent, and C. Lacabanne, *Macromolecules*, **36**, 5187 (2003).
46. M. Jouni, J. Faure-Vincent, P. Fedorko, D. Djurado, G. Boiteux, and V. Massardier, *Carbon*, **76**, 10 (2014).
47. E. Hamciuc, C. Hamciuc, V.E. Musteata, Y. Kalvachev, and A. Wolinska-Grabczyk, *High Perform. Polym*., **26**, 175 (2014).
48. B. Louati, M. Gargouri, K. Guidara, and T. Mhiri, *J. Phys. Chem. Solid*., **66**, 762 (2005).
49. R.H. Chen, R.Y. Chang, and S.C. Shern, *J. Phys. Chem. Solid*., **63**, 2069 (2002).
50. A.N. Papathanassiou, I. Sakellis, and J. Grammatikakis, *Appl. Phys. Lett*., **91**, 122911 (2007).
51. C.R. Cena, A.K. Behera, and B. Behera, *J. Adv. Ceram*., **5**, 84 (2016).
52. S. Dash, R.N.P. Choudhary, P.R. Das, and A. Kumar, *Can. J. Phys*., **93**, 738 (2014).
53. D.K. Pradhan, R.N.P. Choudhary, and B.K. Samantaray, *Express Polym. Lett*., **2**, 630 (2008).